PCCP

Climbing up Conical Intersections: A Direct Dynamics Study of the Exotic Photochemistry of Criegee Intermediates

Journal:	*Physical Chemistry Chemical Physics*
Manuscript ID	CP-ART-04-2022-001860.R2
Article Type:	Paper
Date Submitted by the Author:	15-Jun-2022
Complete List of Authors:	Antwi, Ernest; University of Louisiana at Lafayette Bush, Rachel; University of Louisiana at Lafayette, Marchetti, Barbara; University of Louisiana at Lafayette Karsili, Tolga; university of Louisiana at Lafayette, Chemistry

Climbing up Conical Intersections: A Direct Dynamics Study of the Exotic Photochemistry of Criegee Intermediates

Ernest Antwi, Rachel E. Bush,[#] Barbara Marchetti, and Tolga N. V. Karsili*

University of Louisiana at Lafayette, Lafayette, LA 70503, USA

*Corresponding author's contact detail: tolga.karsili@louisiana.edu

[#]Author contributed as an undergraduate research assistant

Abstract

Criegee intermediates are amongst the most fascinating molecules in modern-day chemistry. They are highly reactive intermediates that find vital roles that range from atmospheric chemistry to organic synthesis. Their excited state chemistry is exotic and complicated, and a myriad of electronic states can contribute to their photodissociation dynamics. This manuscript reports a multi-state direct dynamics (full-dimensional) study of the photoinduced fragmentation of the simplest Criegee intermediate, CH_2OO, using state-of-the-art CASPT2 trajectory surface hopping. Following vertical excitation to the strongly absorbing S_2 ($^1\pi\pi^*$) state , internal conversion, and thus changes in the electronic state character of the separating $O + CH_2O$ fragments, is observed between parent electronic states at separations that, traditionally, might be viewed as the classically asymptotic region of the potential energy surface. We suggest that such long-range internal conversion may account for the unusual and non-intuitive total kinetic energy distribution in the $O(^1D) + H_2CO(S_0)$ products observed following photoexcitation of CH_2OO. The present results also reveal the interplay between seven singlet electronic states and dissociation to yield the experimentally observed $O(^1D) + H_2CO(S_0)$ and $O(^3P) + H_2CO(T_1)$ products. The former (singlet) products are favored, with a branching ratio of ca. 80 %, quantifying the hitherto unknown product branching ratios observed in velocity map imaging experiments. To the best of our knowledge, such long-range internal conversions that lead to changes in the electronic state character of the fragment pairs originating from a common parent

– at classically asymptotic separations – has not been recognized hitherto in the case of a molecular photodissociation.

Introduction

Criegee intermediates (CIs) are carbonyl oxides that have attracted a cornucopia of attention for at least the past 2 decades.[1] They are implicated in enhancing the oxidizing capacity of the troposphere[2–7] and in forming lower volatility products that typically condense to form secondary organic aerosols.[2,8]

Volatile alkenes emitted into the troposphere can undergo reaction with ozone to form a primary ozonide (POZ). The resulting POZ is formed highly internally excited and decays to form aldehyde/ketone and CI products. The latter CI is also formed highly internally excited and may undergo unimolecular decay or collisions with bath atmospheric gases to form a stabilized CI (sCI). The sCI may also undergo unimolecular decay or bimolecular chemistry with trace vapor molecules in the troposphere, e.g., water, alcohols and organic acids.[9,10,19,11–18] The sCI could also undergo UV-excitation within the tropospherically relevant solar irradiance – which is particularly relevant for larger conjugated CIs that derive from biogenic emissions.[20–23]

The photochemistry of CIs represents an intriguing photodissociation problem, as their rich and complicated excited state dynamics pose some interesting questions that are of interdisciplinary relevance to atmospheric chemistry, organic photochemistry and chemical reaction dynamics. The near-UV absorption spectrum of small CIs, such as formaldehyde oxide (CH_2OO) and acetaldehyde oxide (CH_3CHOO), are dominated by a strong $\pi^* \leftarrow \pi$ electron transition.[11,16,17,21,24–27] The resulting $\pi\pi^*$ state undergoes rapid O-O bond fission to form $O(^1D)$ + $H_2CO(S_0)$ and $O(^3P)$ + H_2CO (T_1) products.[21,24] Figure 1(a) presents the total kinetic energy release (TKER) spectra derived from the acquired $O(^1D)$ and $O(^3P)$ velocity map images,

following excitation at λ_{phot} = 350 nm and 330 nm. At both wavelengths, population in both the $O(^1D) + CH_2O(S_0)$ and $O(^3P) + CH_2O\ (T_1)$ product channels are observed, which can be understood by considering the potential energy (PE) profiles along the O-O stretch (R_{OO}) coordinate (in Figure 1(b)). In the latter, the S_1 and S_2 states encounter a crossing with the S_3 and S_4 states at R_{OO} ~ 1.7 Å. This crossing develops into a conical intersection (CoIn) when motions orthogonal to the O-O stretch coordinate are considered. The crossing at R_{OO} ~ 1.7 Å will henceforth be referred to as CoIn1. A further crossing between the S_3/S_4 and S_5/S_6 states (labelled CoIn2) is observed at R_{OO} ~ 2.2 Å. Both CoIn1 and CoIn2 are likely to promote ultrafast internal conversion between the participating states. Following O-O photodissociation, the $S_0 - S_4$ states correlate with $O(^1D) + CH_2O(S_0)$ products, while the S_5 and S_6 states correlate with the $O(^3P) + CH_2O(T_1)$ products. This implies that formation of the $O(^3P) + CH_2O(T_1)$ products requires internal conversion at both CoIn1 and CoIn2 – to S_n states that have n > 2, i.e., higher n than the initially excited S_2 state.

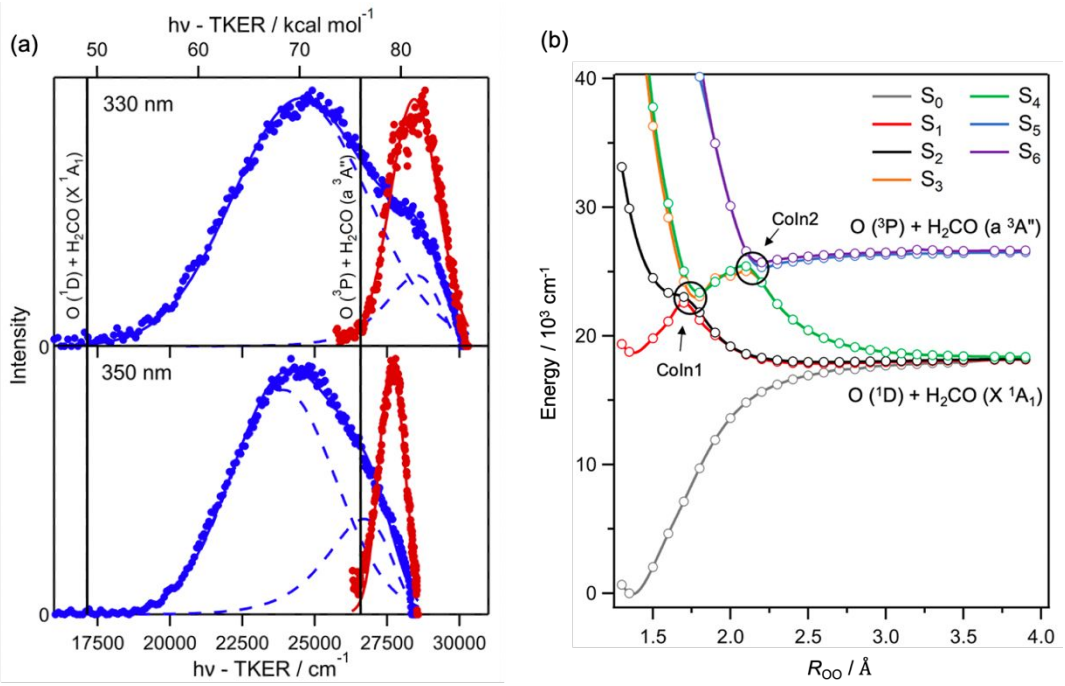

Figure 1: (a) TKER spectra associated with the $O(^3P) + CH_2O$ (blue) and $O(^1D) + CH_2O$ (red) fragments following photoexcitation of CH_2OO at 330 nm (top) and 350 nm (bottom). (b) Adiabatic potential energy profiles of the lowest seven singlet states of CH_2OO along the O-O stretch coordinate. Both (a) and (b) are reproduced with permission from reference 21. We note that the notation used for formaldehyde (CH_2O) in the present study is different from that used in reference 21 (H_2CO).

The excited-state dynamics of CIs show two interesting phenomena: (1) the dynamics involves many electronic states with distinct electronic configurations, which gives rise to a 7-state problem with multi-state intersections; (2) motion through conical intersections to higher lying electronic states than the CoIn, as the excitation energy is sufficient to access the higher lying electronic state. Both phenomena have direct consequences on the electronic state branching into $O(^1D) + CH_2O(S_0)$ and $O(^3P) + CH_2O$ (T_1) products and modelling the evolving dynamics requires (1) an accurate multi-reference method with dynamic correlation, (2) full-dimensionality, and (3) the inclusion of all seven singlet electronic states.

Prior studies have attempted to quantify the inherent product branching ratios into $O(^1D) + CH_2O(S_0)$ and $O(^3P) + CH_2O$ (T_1) products using a range of time-dependent methods. The work by Samanta et al. was the first attempt to quantify the branching ratio into $O(^1D) + CH_2O(S_0)$ and $O(^3P) + CH_2O$ (T_1) products upon photodissociation of CH_2OO.[28] The study involved time-dependent quantum wavepacket propagation, on a reduced dimensional potential energy surface calculated using the Dynamically-Weighted Complete Active Space Self-Consistent Field (DW-CASSCF) method. That study predicted a significant product population inversion favoring $O(^3P) + CH_2O$ (T_1) products. Although informative, the DW-CASSCF method used in that study does not adequately capture the significant dynamic correlation required for describing the photodynamics of CH_2OO. A more recent study used combined experimental and theoretical approaches to study the photodissociation dynamics of CH_2OO.[21]

Surface hopping was used to quantify the branching ratios into the $O(^1D) + CH_2O(S_0)$ and $O(^3P) + CH_2O(T_1)$ products, wherein energies and gradients were calculated "on-the-fly" at the state-averaged-CASSCF level-of-theory. This latter study revealed a preference for the lower energy $O(^1D) + CH_2O(S_0)$ channel. This latter observation is more intuitive on energetic grounds, but since CASSCF was used the absolute branching ratios are only qualitatively correct. Higher level CASPT2 PE profiles of CH_2OO along R_{OO} shows some differences in the topologies when compared to CASSCF PE profiles.[21] This observation suggests that dynamic electron correlation is important in accurately capturing the photodissociation dynamics of CH_2OO.

A somewhat more subtle phenomena is observed in the experimentally measured TKER spectra assigned to $O(^1D) + CH_2O(S_0)$ products – i.e., the blue distribution in Fig. 1(a). The broad TKER distribution reveals a low TKER shoulder that coincidently sits beneath the TKER distribution corresponding to $O(^3P) + CH_2O(T_1)$ products. This slow TKER shoulder is most pronounced in the 330 nm TKER distribution in Figure 1(a), at $h\nu$ – TKER ~ 80 kcal mol^{-1} in the blue distribution. The earlier interpretation[21] of this phenomenon suggested that the evolving population on the S_5 and S_6 states are initially en route to forming $O(^3P) + CH_2O(T_1)$ products but non-adiabatic coupling at Coln2 leads to internal conversion to the S_4 or S_5 state – ultimately forming $O(^1D) + CH_2O(S_0)$ products.

This study reports the 7-state, full-dimensional trajectory surface hopping (TSH) dynamics of photoexcited CH_2OO at the multi-state (MS)-CASPT2 level of theory, thus providing an accurate full-dimensional study of the photodissociation dynamics of CH_2OO. We provide new insights on the branching fractions between the $O(^1D) + CH_2O(S_0)$ and $O(^3P) + CH_2O(T_1)$ products and show that the low-TKER shoulder in the $O(^1D) + CH_2O(S_0)$ distribution may be due to internal conversion between asymptotic electronic states.

Results and Discussion

Fig. 2 presents the minimum energy geometry of CH_2OO which, as previously reported, contains a planar equilibrium geometry. Fig. 2 also presents the orbitals and orbital promotions associated with excitation to the S_1 and S_2 states. Although these transitions are now well-known in the context of CH_2OO,[15,17,21,26,27,29] we reproduce it here to set the scene for the evolving narrative. As Fig. 2 shows, excitation to the S_1 and S_2 states involve $\pi \leftarrow n$ and $\pi^* \leftarrow \pi$ electron promotions, respectively. As previously reported, only the S_2 state contains sufficient oscillator strength in the near-UV.

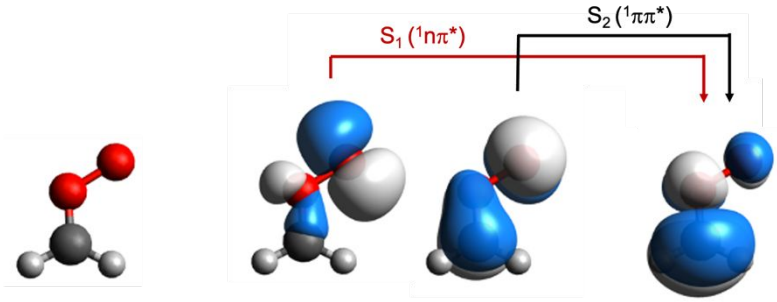

Figure 2: Equilibrium geometry of CH_2OO and the orbital promotions associated with excitation to the S_1 and S_2 states.

Following near-UV excitation, velocity map imaging (VMI) experiments show $O(^1D)$ and $O(^3P)$ atom products – but with little knowledge of the branching fractions into each electronic state. Our TSH simulations provide branching ratios associated with $O(^1D)$ and $O(^3P)$ atom formation as described below.

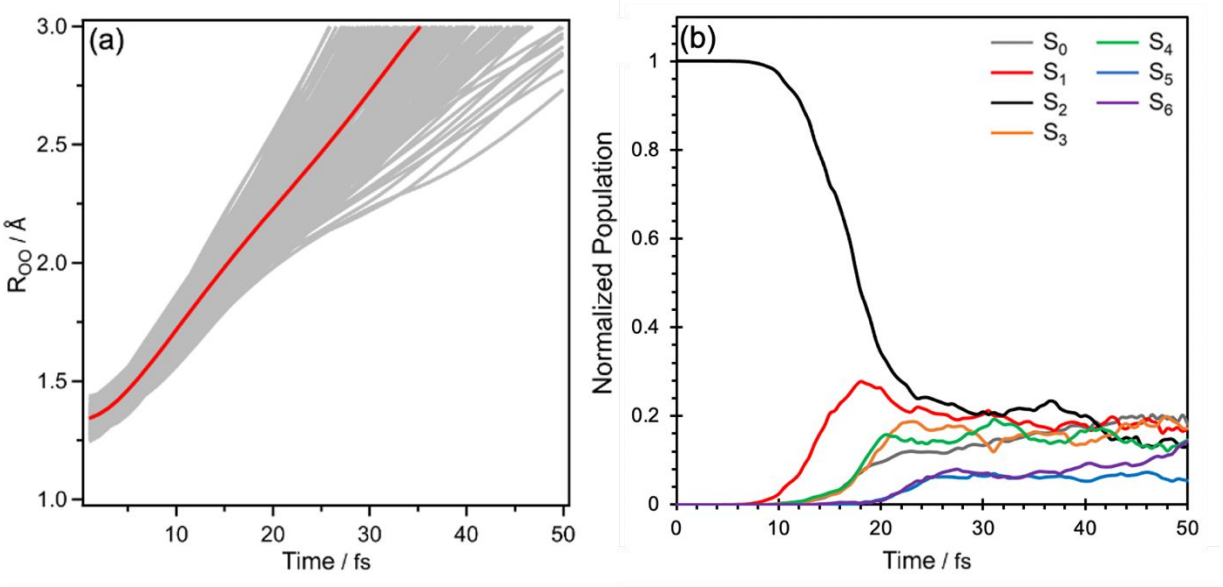

Figure 3: (a) the average (red) and individual trajectory (gray) O-O bond distances as a function of time. (b) Population in the S_0, S_1, S_2, S_3, S_4, S_5, and S_6 states as a function of time as returned from the CASPT2 trajectories.

As Figure 3(a) shows, all trajectories that were initiated on the bright S_2 state undergo rapid bond elongation to an asymptotic R_{OO} value – which, as guided by the PE profiles in Figure 1(b), is taken to be 3 Å. This implies that photoinduced O-O bond fission is prompt and occurs on timescale <100 fs and with unity quantum yield. This is in excellent agreement with the translationally excited O-atom products and their limiting recoil anisotropy parameter observed in VMI studies.[21] The latter observation indicates that the O-O bond fission occurs on timescales that are substantially shorter than molecular rotation.

At this point, our results indicate that O-O bond fission occurs on an ultrashort timescale. Of greater importance is the question: what path does the evolving dynamics follow to form O + CH_2O products? Figure 3(b) provides such answers, which presents the normalized population as a function of time from the MS-CASPT2 surface hopping results. As shown, the initially prepared S_2 state starts to depopulate at ca. 8 fs, undergoing initial internal conversion to the S_1

state in 8-15 fs and to the S_3 and S_4 pair of states in 10 – 20 fs. At >40 fs, where all trajectories have reached long R_{OO} bond distances, the surface hopping results indicate that ca. 20 % of the population remains on the S_5 and S_6 states – corresponding to $O(^3P) + CH_2O(T_1)$ products. The remaining 80 % are distributed among the $S_0 – S_4$ states, which correspond to $O(^1D) + CH_2O(S_0)$ products. This indicates that only ca. 20 % of the initially excited CH_2OO molecules dissociate to form $O(^3P) + CH_2O(T_1)$ products, while the remaining 80 % partition to form $O(^1D) + CH_2O(S_0)$ products within 50 fs.

The most striking observations returned from our TSH simulations are the hops from the S_5 and S_6 states at long R_{OO} values – i.e., in regions of configuration space that are classically asymptotic along the O-O dissociation coordinate. Fig. 4 presents the CO distances (R_{CO}) and HCO angles (A_{HCO}) at which hops from the S_5 and S_6 states to the S_0, S_1, S_2, S_3 or S_4 states occur at $R_{OO} > 3$ Å. This value of R_{OO} is chosen since it is the distance at which the energy profile along the O-O coordinate becomes asymptotic. Observation of surface hops from the S_5/S_6 states implies non-adiabatic coupling between electronic states that correlate with $O(^1D) + CH_2O(S_0)$ and $O(^3P) + CH_2O(T_1)$ products at R_{OO} distances that would otherwise be considered classically asymptotic – i.e., where the CH_2O + O fragments have minimal interaction. As Fig. 4 shows, the geometry of the CH_2O (i.e., formaldehyde) counter-fragment at these hopping points are mostly with HCO angles that are smaller, and CO bond distances that are longer, than their equilibrium values in the parent CH_2OO and formaldehyde (T_1) molecules. These results indicate that R_{CO} and A_{HCO} motions in the CH_2O counter-fragment lead to spin-allowed internal conversion in CH_2OO, between electronic states that correlate with $O(^3P) + CH_2O(T_1)$ products (S_6 and S_5) to those that correlate with $O(^1D) + CH_2O(S_0)$ products (S_4, S_3, S_2, S_1 and S_0) at R_{OO} distances that might be viewed as the classically asymptotic region of the potential energy surface along the

dissociation coordinate. To the best of our knowledge, this long-range internal conversion is a hitherto unrecognized phenomena in molecular photodissociation and arises from degeneracies between the S_0, S_1, S_2, S_3, S_4, S_5 and S_6 states at long R_{OO}. This is seen clearly in Fig. S3 of the supporting information which shows an energy vs. time plot of a representative trajectory that undergoes such long-range hopping from the S_5/S_6 state. Since the motions that such long-range degeneracies are centered on the formaldehyde co-fragment this motivates us to explore the energy profiles along the R_{CO} and A_{HCO} coordinates in CH_2O in more detail.

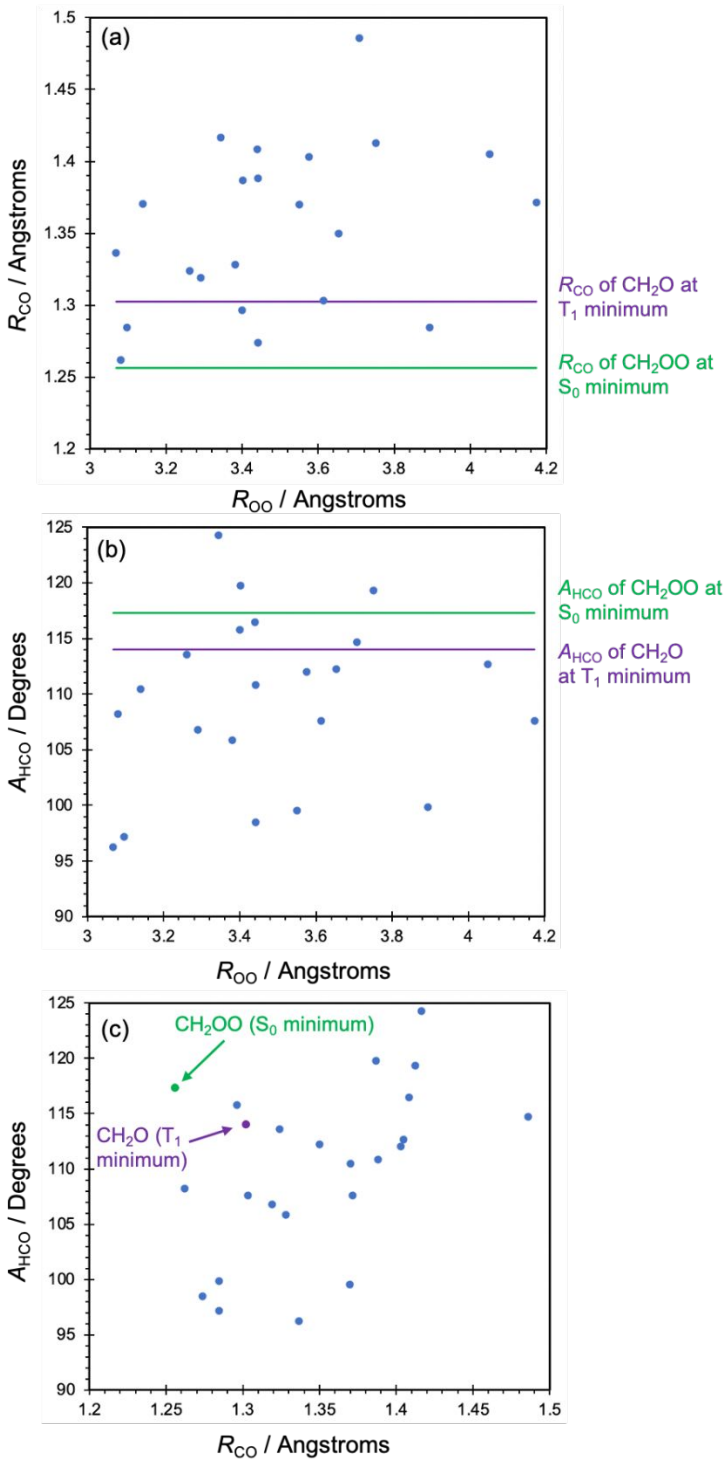

Figure 4: The R_{CO} and A_{HCO} values of CH_2OO at which hops from the S_5 and S_6 states to either of the S_n states (where $n \leq 4$) occur at R_{OO} distances longer than 3 Å. (a) Shows R_{CO} and R_{OO} values of the long-range hops from the S_5/S_6 states of CH_2OO. (b) Shows the A_{HCO} and R_{OO} values of the long-range hops from the S_5/S_6 states of CH_2OO. The green and purple lines show the equilibrium A_{HCO} values in, respectively, the parent CH_2OO (S_0) and formaldehyde (T_1). (c) presents the A_{HCO} and R_{CO} values of the long-range hops from the S_5/S_6 states of CH_2OO at R_{OO}

> 3 Å. The green and purple points (and lines) represent the R_{CO} and R_{HCO} values of, respectively, the parent CH_2OO (S_0) and formaldehyde (T_1).

Fig. 5 presents the relaxed PE profiles along the A_{HCO} and R_{CO} coordinates of formaldehyde (CH_2O). These calculations are undertaken by fixing either A_{HCO} or R_{CO} coordinate of formaldehyde at various values and allowing the remainder of the nuclear framework to relax to their B3LYP/cc-pVTZ minimum energy geometry. These relaxed scans are undertaken for both the S_0 and T_1 states of formaldehyde. Single point CASPT2/aug-cc-pVTZ calculations are then undertaken on the returned B3LYP/cc-pVTZ relaxed PE points. In all cases the S_0 state is shifted by an amount equivalent to the experimentally measured $O(^3P)$-$O(^1D)$ energy splitting (15780 cm^{-1}/1.96 eV)[30] which we label as "S_0(shift)" in the PE profiles in Fig. 5. S_0(shift) directly relates to the $O(^1D) + CH_2O(S_0)$ energetic limit of CH_2OO at long R_{OO}. When viewed from this perspective, the unshifted S_0 state directly relates to the lowest energy (spin-forbidden) $O(^3P) + CH_2O(S_0)$ product channel. The T_1 states in Fig. 5 then directly relate to the spin-allowed $O(^3P) + CH_2O(T_1)$ channel with no equivalent energy shift required since the O atom remains in its lowest energy electronic configuration. Changes in the S_0(shift) and T_1 state energies, via nuclear motions along the A_{CHO} and R_{CO} coordinates, are therefore analogous to energy changes along the equivalent coordinates in, respectively, the $S_0/S_1/S_2/S_3/S_4$ and S_5/S_6 states of CH_2OO at asymptotic R_{OO} distances. Degeneracies between the S_0(shift) and T_1 states therefore represent equivalent degeneracies that would be expected between the $S_0/S_1/S_2/S_3/S_4$ and S_5/S_6 states of CH_2OO at long R_{OO}. Since such degeneracies are solely due to nuclear motions of CH_2O, the S_0(shift) and T_1 PE profiles in Fig. 5 directly relate to the CH_2OO molecule at long R_{OO} and represent the necessary nuclear motions that promote internal conversion at asymptotic regions of the PE surface configuration space.

Figs. 5 (a) and (b) present the CASPT2/aug-cc-pVTZ//B3LYP/cc-pVTZ PE profiles along the A_{HCO} coordinate for, respectively, the relaxed S_0 and T_1 electronic states of formaldehyde. As shown in Fig. 5(b), the T_1 minimum of formaldehyde is pyramidal. Motion along A_{HCO} leads to degeneracies between the S_0(shift) and T_1 states – implying that an equivalent spin allowed crossing occurs in CH_2OO between the electronic states that correlate with the $O(^1D)$ + $CH_2O(S_0)$ and $O(^3P)$ + $CH_2O(T_1)$ limits at long R_{OO}. These degeneracies are analogous to the long R_{OO} hops from the S_5 and S_6 states observed in the TSH simulations, which are mostly at A_{HCO} values that are smaller than the equivalent angle in the minimum energy geometry of CH_2OO (S_0) and CH_2O (T_1).

Additionally, Figs. 5(c) and 5(d) shows equivalent crossings along the R_{CO} coordinate. This is most noticeable in Fig. 5(d) which shows a crossing between the shifted S_0 PE profile and the T_1 relaxed profile at a slight CO elongation from the $CH_2O(T_1)$ equilibrium geometry. Again, this accounts for the long R_{OO} hops from S_5 and S_6 states at R_{CO} values that are somewhat longer than the equivalent R_{CO} values in the minimum energy geometry of $CH_2OO(S_0)$ and CH_2O (T_1).

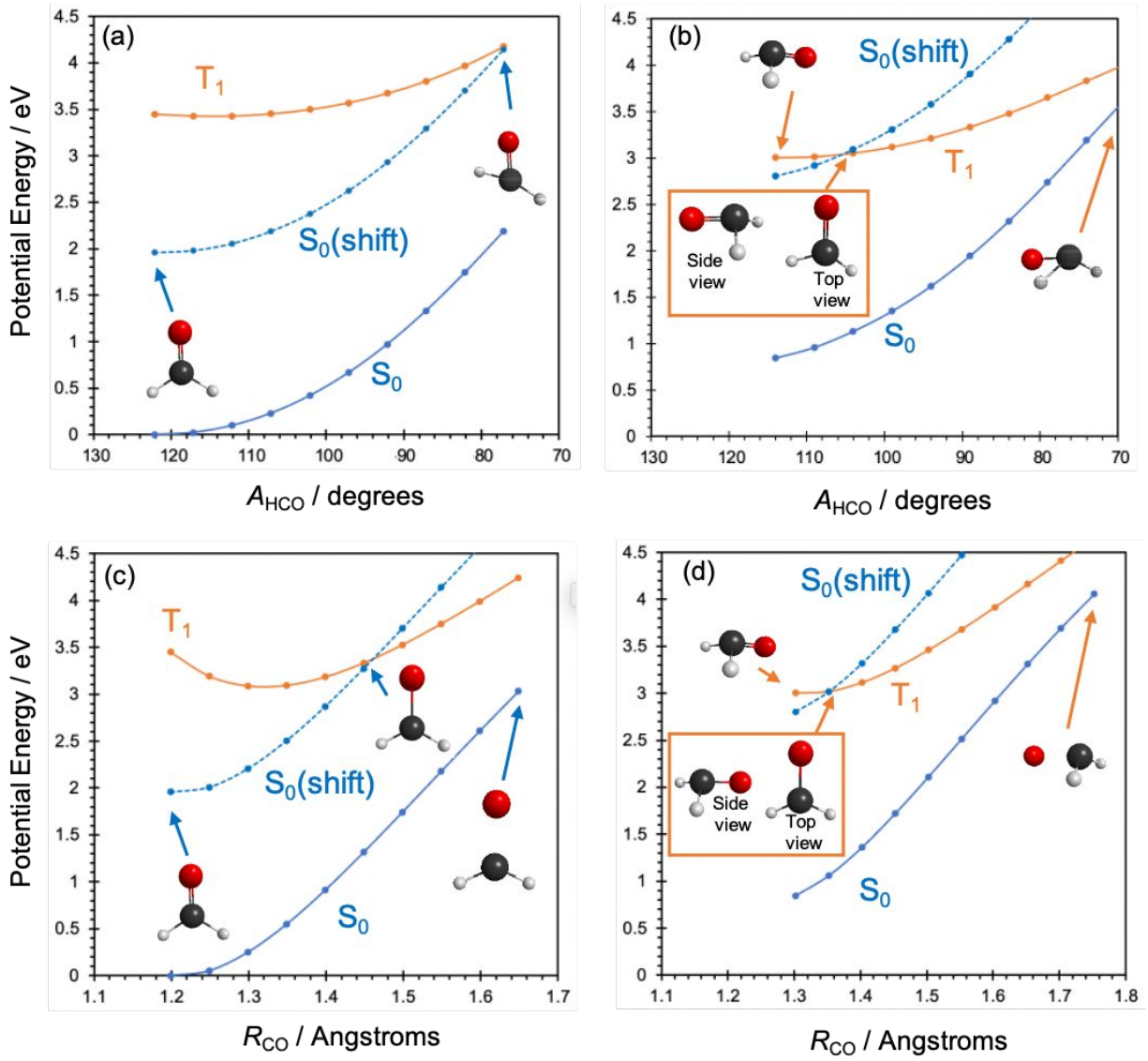

Figure 5: CASPT2(6,5)/aug-cc-pVTZ PE profiles of formaldehyde (CH_2O) along the A_{HCO} [(a) and (b)] and R_{CO} [(c) and (d)] coordinates. Panels (a) and (c) correspond to, respectively, the relaxed S_0 PE profiles along the A_{HCO} and R_{CO} coordinates and the corresponding T_1 energies at the corresponding S_0 relaxed geometry. The dotted blue profile (labelled S_0(shift)) corresponds to the S_0 profile shifted by 1.96 eV (i.e., the $O(^1D) - O(^3P)$ energy gap) to match the experimental $O(^1D) + CH_2O(S_0)$ asymptote. Panels (b) and (d) correspond to, respectively, the relaxed T_1 PE profiles along the A_{HCO} and R_{CO} coordinates and the corresponding S_0 energies at the corresponding T_1 relaxed geometry. Again, the dotted blue profile (labelled S_0(shift)) corresponds to the S_0 profile shifted by 1.96 eV (i.e., the $O(^1D) - O(^3P)$ energy gap) to match the experimental $O(^1D) + CH_2O(S_0)$ asymptote.

Given these hops and degeneracies at asymptotic distances, the low TKER edge of the $O(^1D)$ + $CH_2O(S_0)$ distribution at hν – TKER ~ 80 kcal mol^{-1} may be a result of this long-range internal conversion, wherein the evolving S_5/S_6 population en route to forming internally cold $CH_2O(T_1)$ + $O(^3P)$ products undergoes long-range spin allowed internal conversion to S_4, S_3, S_2, S_1 or S_0 states, ultimately forming $CH_2O(S_0)$ + $O(^1D)$ products. Since the internal conversion occurs from higher energy states, the subsequent $CH_2O(S_0)$ is formed highly internally excited which manifests in translationally slower $O(^1D)$ fragments. This would then manifest in a low TKER shoulder that is distinct from the $CH_2O(S_0)$ + $O(^1D)$ TKER distribution formed from direct dissociation on the S_4, S_3, S_2, S_1 or S_0 states.

Conclusions and Outlook

We have performed a multi-reference direct dynamics study of the full-dimensional multi-state photodissociation dynamics of the simplest Criegee intermediate, CH_2OO, using MS-CASPT2 surface hopping molecular dynamics simulations. The results have significance to the fields of atmospheric chemistry, photochemical synthesis, and chemical reaction dynamics.

We have shown that the initially prepared S_2 state of CH_2OO undergoes prompt O-O bond fission within 50 fs. Within this short timescale, internal conversion among the seven electronic states controls the electronic state branching into the $O(^1D)$ + $CH_2O(S_0)$ and $O(^3P)$ + $CH_2O(T_1)$ product channels – with the former dominating with ca. 80 % of the overall quantum yield.

Our results also reveal long-range internal conversion, at areas of the PE surface that traditionally mighe be view as classically asymptotic. To the best of our knowledge, such behavior is hitherto unobserved in a photodissociation case. The results may have profound atmospheric consequences – such as CIs potentially contributing to the day-time budget of $O(^1D)$

and O(^{3}P) atoms – which are important atmospheric species. Notably, O(^{1}D) reacts rapidly with water vapor to form OH radicals. Photoexcitation of CIs may therefore contribute to the oxidizing capacity of the troposphere. This may be particularly true for larger and more functionalized CIs that have electronic absorption spectra that align better with the tropospherically relevant solar irradiance profile. The results may also have consequences for synthetic chemistry wherein Criegee intermediates are important precursors.[31–35] *In situ* photochemical trapping of these species may provide a route for forming aldehyde or ketone species with high yield.

Moving forward, we are excited to explore how the photodissociation dynamics change upon increasing CI molecular complexity, where we look forward to extending the current study to isoprene and α-pinene derived Criegee intermediates.

Computational Methodology

The ground state equilibrium geometry of CH_2OO was optimized at the B2PLYP-D3/cc-pVTZ level of theory.[36,37] This functional and basis set combination has been shown to perform well for determining geometries and normal modes of CIs[21,23,27,38] and for consistency when comparing the resulting dynamics with prior work.[21] Trajectory surface hopping (TSH) simulations were performed using the surface hopping method with quantum transitions of Hammes-Schiffer and Tully[39] as implemented in Newton-X.[40,41] Initial positions and momenta were obtained by means of a Wigner distribution based on the B2PLYP-D3/cc-pVTZ equilibrium geometry and associated harmonic normal mode wavenumbers. In the TSH simulations, the nuclear coordinates were propagated by integrating Newton's equation using the velocity Verlet method, while the electronic coordinates were propagated by numerically solving the time-dependent

Schrödinger equation using Butcher's fifth-order Runge-Kutta method in steps of 0.025 fs.[42] Trajectories were initiated in the S_2 state and the energies and gradients of the seven lowest singlet states were calculated "on-the-fly" using the single-state, single-reference multistate complete active space second order perturbation theory (SS-SR-CASPT2) method in conjunction with the cc-pVDZ basis set.[43] SS-SR-CASPT2 enables the computation of energies and analytical gradients at MS-CASPT2 quality, at a reduced computational cost; it also performs well near electronic state degeneracies. The SS-SR-CASPT2 calculations were based on a state-averaged complete active space self-consistent field (CASSCF) method reference wavefunction and an active space comprising 10 electrons in 8 orbitals as depicted in Fig. S1 of the supporting information. These were performed via the BAGEL interface to Newton-X.[44] The state hopping probabilities were evaluated by calculating the non-adiabatic coupling matrix elements from the SS-SR-CASPT2 computations. 199 trajectories were propagated in time with a step size of 0.5 fs.

Additional calculations were carried out on formaldehyde (CH_2O). The equilibrium geometry of the S_0 and T_1 states of CH_2O were optimized at the B3LYP/cc-pVTZ level of theory. The resulting geometries were used to undertake B3LYP/cc-pVTZ relaxed scans along the CO stretch and HCO bend of formaldehyde. Single point energies at the CASPT2/aug-cc-pVTZ level of theory were computed on the resulting B3LYP/cc-pVTZ relaxed geometries. The B3LYP functional allows for stable computation of the relaxed structures while minimizing computational expense. Additionally, bare CASPT2 – as opposed to MS-CASPT2 – is adequate since no electronic state degeneracies are returned along the scan coordinate – as confirmed by the comparison between the bare CASPT2 and SS-SR-CASPT2 benchmarks in the supporting information. These computations were based on an active space of 6 electrons in 5 orbitals as

depicted in Fig. S2 and involved a state-averaged reference wavefunction comprising only the S_0 and T_1 states of CH_2O.

All CASPT2 calculations used an imaginary level shift of 0.5 E_H to aid convergence and circumvent intruder state effects. The density functional theory (B2PLYP-D3 and B3LYP) computations were carried out using Gaussian 16,[45] while the CASPT2 single point energy calculations were carried out in Molpro.[46,47]

Acknowledgements

The work reported here is supported by the National Science Foundation, under Grant no. 2003422. Portions of this research were conducted with high performance computational resources provided by the Louisiana Optical Network Infrastructure (http://www.loni.org).

References

1 N. M. Donahue, G. T. Drozd, S. A. Epstein, A. A. Presto and J. H. Kroll, Adventures in ozoneland: Down the rabbit-hole, *Phys. Chem. Chem. Phys.*, 2011, **13**, 10848–10857.

2 D. Johnson and G. Marston, The gas-phase ozonolysis of unsaturated volatile organic compounds in the troposphere, *Chem. Soc. Rev.*, 2008, **37**, 699–716.

3 K. M. Emmerson and N. Carslaw, Night-time radical chemistry during the TORCH campaign, *Atmos. Environ.*, 2009, **43**, 3220–3226.

4 K. M. Emmerson, N. Carslaw, D. C. Carslaw, J. D. Lee, G. McFiggans, W. J. Bloss, T. Gravestock, D. E. Heard, J. Hopkins, T. Ingham, M. J. Pilling, S. C. Smith, M. Jacob and P. S. Monks, Free radical modelling studies during the UK TORCH Campaign in Summer 2003, *Atmos. Chem. Phys.*, 2007, **7**, 167–181.

5 M. S. Alam, M. Camredon, A. R. Rickard, T. Carr, K. P. Wyche, K. E. Hornsby, P. S. Monks and W. J. Bloss, Total radical yields from tropospheric ethene ozonolysis, *Phys. Chem. Chem. Phys.*, 2011, **13**, 11002–11015.

6 M. S. Alam, A. R. Rickard, M. Camredon, K. P. Wyche, T. Carr, K. E. Hornsby, P. S. Monks and W. J. Bloss, Radical product yields from the ozonolysis of short chain alkenes under atmospheric boundary layer conditions, *J. Phys. Chem. A*, 2013, **117**, 12468–12483.

7 A. S. Hasson, G. Orzechowska and S. E. Paulson, Production of stabilized Criegee intermediates and peroxides in the gas phase ozonolysis of alkenes 1. Ethene, trans-2-butene, and 2,3-dimethyl-2-butene, *J. Geophys. Res. Atmos.*, 2001, **106**, 34131–34142.

8 D. Meidan, J. S. Holloway, P. M. Edwards, W. P. Dubé, A. M. Middlebrook, J. Liao, A. Welti, M. Graus, C. Warneke, T. B. Ryerson, I. B. Pollack, S. S. Brown and Y. Rudich, Role of Criegee Intermediates in Secondary Sulfate Aerosol Formation in Nocturnal Power Plant Plumes in the Southeast US, *ACS Earth Sp. Chem.*, 2019, **3**, 748–759.

9 A. W.-L. L. Ting and J. J.-M. M. Lin, UV Spectrum of the Simplest Deuterated Criegee Intermediate CD2OO, *J. Chinese Chem. Soc.*, 2017, **64**, 360–368.

10 Y. P. Chang, Y. L. Li, M. L. Liu, T. C. Ou and J. J. M. Lin, Absolute Infrared Absorption Cross Section of the Simplest Criegee Intermediate Near 1285.7 cm-1, *J. Phys. Chem. A*, 2018, **122**, 8874–8881.

11 W. L. Ting, Y. H. Chen, W. Chao, M. C. Smith and J. J. M. Lin, The UV absorption spectrum of the simplest Criegee intermediate CH 2OO, *Phys. Chem. Chem. Phys.*, 2014, **16**, 10438–10443.

12 M. C. Smith, W. L. Ting, C. H. Chang, K. Takahashi, K. A. Boering and J. J. M. Lin, UV absorption spectrum of the C2 Criegee intermediate CH3CHOO, *J. Chem. Phys.*, ,

DOI:10.1063/1.4892582.

13 Y.-P. P. Chang, C.-H. H. Chang, K. Takahashi and J. J.-M. M. Lin, Absolute UV absorption cross sections of dimethyl substituted Criegee intermediate (CH3)2COO, *Chem. Phys. Lett.*, 2016, **653**, 155–160.

14 L. Sheps, A. M. Scully and K. Au, UV absorption probing of the conformer-dependent reactivity of a Criegee intermediate CH3CHOO, *Phys. Chem. Chem. Phys.*, 2014, **16**, 26701–26706.

15 L. Sheps, Absolute Ultraviolet Absorption Spectrum of a Criegee Intermediate CH 2OO, *J. Phys. Chem. Lett.*, 2013, **4**, 4201–4205.

16 Sršeň, D. Hollas and P. Slavíček, UV absorption of Criegee intermediates: Quantitative cross sections from high-level: Ab initio theory, *Phys. Chem. Chem. Phys.*, 2018, **20**, 6421–6430.

17 R. Dawes, B. Jiang and H. Guo, UV absorption spectrum and photodissociation channels of the simplest criegee intermediate (CH2OO), *J. Am. Chem. Soc.*, 2015, **137**, 50–53.

18 P. Aplincourt, E. Henon, F. Bohr and M. F. Ruiz-López, Theoretical study of photochemical processes involving singlet excited states of formaldehyde carbonyl oxide in the atmosphere, *Chem. Phys.*, 2002, **285**, 221–231.

19 E. S. Foreman, K. M. Kapnas, Y. T. Jou, J. Kalinowski, D. Feng, R. B. Gerber and C. Murray, High resolution absolute absorption cross sections of the B1A′-X1A′ transition of the CH2OO biradical, *Phys. Chem. Chem. Phys.*, 2015, **17**, 32539–32546.

20 M. F. Vansco, B. Marchetti and M. I. Lester, Electronic spectroscopy of methyl vinyl ketone oxide: A four-carbon unsaturated Criegee intermediate from isoprene ozonolysis, *J. Chem. Phys.*, 2018, **149**, 244309.

21 V. J. Esposito, T. Liu, G. Wang, A. Caracciolo, M. F. Vansco, B. Marchetti, T. N. V. Karsili and M. I. Lester, Photodissociation Dynamics of CH2OO on Multiple Potential Energy Surfaces: Experiment and Theory, *J. Phys. Chem. A*, 2021, **125**, 6571–6579.

22 M. F. Vansco, B. Marchetti, N. Trongsiriwat, T. Bhagde, G. Wang, P. J. Walsh, S. J. Klippenstein and M. I. Lester, Synthesis, Electronic Spectroscopy, and Photochemistry of Methacrolein Oxide: A Four-Carbon Unsaturated Criegee Intermediate from Isoprene Ozonolysis, *J. Am. Chem. Soc.*, 2019, **141**, 15058–15069.

23 G. Wang, T. Liu, A. Caracciolo, M. F. Vansco, N. Trongsiriwat, P. J. Walsh, B. Marchetti, T. N. V Karsili and M. I. Lester, Photodissociation dynamics of methyl vinyl ketone oxide: A four-carbon unsaturated Criegee intermediate from isoprene ozonolysis., *J. Chem. Phys.*, 2021, **155**, 174305.

24 J. M. Beames, F. Liu, L. Lu and M. I. Lester, Ultraviolet spectrum and photochemistry of the simplest criegee intermediate CH2OO, *J. Am. Chem. Soc.*, 2012, **134**, 20045–20048.

25 L. Sheps, B. Rotavera, A. J. Eskola, D. L. Osborn, C. A. Taatjes, K. Au, D. E. Shallcross, M. A. H. Khan and C. J. Percival, The reaction of Criegee intermediate CH2OO with water dimer: Primary products and atmospheric impact, *Phys. Chem. Chem. Phys.*, 2017, **19**, 21970–21979.

26 V. J. Esposito, O. Werba, S. A. Bush, B. Marchetti and T. N. V. Karsili, Insights into the Ultrafast Dynamics of CH2OO and CH3CHOO Following Excitation to the Bright 1ππ* State: The Role of Singlet and Triplet States, *Photochem. Photobiol.*, , DOI:10.1111/php.13560.

27 J. C. McCoy, B. Marchetti, M. Thodika and T. N. V. Karsili, A Simple and Efficient Method for Simulating the Electronic Absorption Spectra of Criegee Intermediates:

Benchmarking on CH2OO and CH3CHOO, *J. Phys. Chem. A*, 2021, **125**, 4089–4097.

28 K. Samanta, J. M. Beames, M. I. Lester and J. E. Subotnik, Quantum dynamical investigation of the simplest Criegee intermediate CH2OO and its O-O photodissociation channels, *J. Chem. Phys.*, 2014, **141**, 134303.

29 J. H. Lehman, H. Li, J. M. Beames and M. I. Lester, Communication: Ultraviolet photodissociation dynamics of the simplest Criegee intermediate CH2OO, *J. Chem. Phys.*, 2013, **139**, 141103.

30 A. Kramida, Y. Ralchenko, J. Reader and NIST ASD Team, NIST Atomic Spectra Database (ver. 5.1), National Institute of Standards and Technology, Gaithersburg, MD, 10 September 2014,.

31 W. W. Sander, P-Benzoquinone O-oxide, *J. Org. Chem.*, 1988, **53**, 2091–2093.

32 W. Sander, Carbonyl Oxides: Zwitterions or Diradicals?, *Angew. Chemie Int. Ed. English*, 1990, **29**, 344–354.

33 C. Geletneky and S. Berger, The mechanism of ozonolysis revisited by 17O-NMR spectroscopy, *European J. Org. Chem.*, 1998, **1998**, 1625–1627.

34 O. Horie and G. K. Moortgat, Decomposition pathways of the excited Criegee intermediates in the ozonolysis of simple alkenes, *Atmos. Environ. Part A, Gen. Top.*, 1991, **25**, 1881–1896.

35 B. E. Coleman and B. S. Ault, Investigation of the thermal and photochemical reactions of ozone with styrene in argon and krypton matrices, *J. Mol. Struct.*, 2012, **1023**, 81–86.

36 S. Grimme, Semiempirical hybrid density functional with perturbative second-order correlation, *J. Chem. Phys.*, 2006, **124**, 34108.

37 T. H. Dunning, Gaussian basis sets for use in correlated molecular calculations. I. The

atoms boron through neon and hydrogen, *J. Chem. Phys.*, 1989, **90**, 1007–1023.

38 V. P. Barber, S. Pandit, A. M. Green, N. Trongsiriwat, P. J. Walsh, S. J. Klippenstein and M. I. Lester, Four-Carbon Criegee Intermediate from Isoprene Ozonolysis: Methyl Vinyl Ketone Oxide Synthesis, Infrared Spectrum, and OH Production, *J. Am. Chem. Soc.*, 2018, **140**, 10866–10880.

39 S. Hammes-Schiffer and J. C. Tully, Proton transfer in solution: Molecular dynamics with quantum transitions, *J. Chem. Phys.*, 1994, **101**, 4657–4667.

40 M. Barbatti, G. Granucci, M. Persico, M. Ruckenbauer, M. Vazdar, M. Eckert-Maksić and H. Lischka, The on-the-fly surface-hopping program system Newton-X: Application to ab initio simulation of the nonadiabatic photodynamics of benchmark systems, *J. Photochem. Photobiol. A Chem.*, 2007, **190**, 228–240.

41 M. Barbatti, M. Ruckenbauer, F. Plasser, J. Pittner, G. Granucci, M. Persico and H. Lischka, Newton-X: a surface-hopping program for nonadiabatic molecular dynamics, *Wiley Interdiscip. Rev. Comput. Mol. Sci.*, 2013, **4**, 26–33.

42 J. C. Butcher, A Modified Multistep Method for the Numerical Integration of Ordinary Differential Equations, *J. ACM*, 1965, **12**, 124–135.

43 J. W. Park and T. Shiozaki, Analytical Derivative Coupling for Multistate CASPT2 Theory, *J. Chem. Theory Comput.*, 2017, **13**, 2561–2570.

44 T. Shiozaki, BAGEL: Brilliantly Advanced General Electronic-structure Library, *Wiley Interdiscip. Rev. Comput. Mol. Sci.*, 2018, **8**, e1331.

45 and D. J. F. , M. J. Frisch, G. W. Trucks, H. B. Schlegel, G. E. Scuseria, M. A. Robb, J. R. Cheeseman, G. Scalmani, V. Barone, G. A. Petersson, H. Nakatsuji, X. Li, M. Caricato, A. V. Marenich, J. Bloino, B. G. Janesko, R. Gomperts, B. Mennucci, H. P. Hratchian, J.

V, Gaussian 16, Revision C.01, *Gaussian Inc. Wallingford CT*.

46 H.-J. Werner, P. J. Knowles, G. Knizia, F. R. Manby, M. Schütz, P. Celani, W. Györffy, D. Kats, T. Korona, R. Lindh, A. Mitrushenkov, G. Rauhut, K. R. Shamasundar, T. B. Adler, R. D. Amos, S. Bennie, A. Bernhardsson, A. Berning, D. L. Cooper, M. J. O. Deegan, A. J. Dobbyn, F. Eckert, E. Goll, C. Hampel, A. Hesselmann, G. Hetzer, T. Hrenar, G. Jansen, C. Köppl, S. J. R. Lee, Y. Liu, A. W. Lloyd, Q. Ma, R. A. Mata, A. J. May, S. J. McNicholas, W. Meyer, T. F. M. III, M. E. Mura, A. Nicklass, D. P. O'Neill, P. Palmieri, D. Peng, K. Pflüger, R. Pitzer, M. Reiher, T. Shiozaki, H. Stoll, A. J. Stone, R. Tarroni, T. Thorsteinsson, M. Wang and M. Welborn, MOLPRO, version 2018.1, a package of ab initio programs.

47 H.-J. Werner, P. J. Knowles, G. Knizia, F. R. Manby and M. Schütz, Molpro: a general-purpose quantum chemistry program package, *WIREs Comput. Mol. Sci.*, 2012, **2**, 242–253.